# Functionalized multiwalled carbon nanotubes as ultrasound contrast agents

Lucia Gemma Delogu[a,1], Gianpaolo Vidili[b], Enrica Venturelli[c], Cécilia Ménard-Moyon[c], Maria Antonietta Zoroddu[a], Giovannantonio Pilo[d], Paola Nicolussi[d], Ciriaco Ligios[d], Davide Bedognetti[e,f], Francesco Sgarrella[a], Roberto Manetti[b], and Alberto Bianco[c,1]

[a]Dipartimento di Chimica e Farmacia and [b]Dipartimento di Medicina Clinica, Sperimentale e Oncologica, Università degli Studi di Sassari, 07100 Sassari, Italy; [c]Centre National de la Recherche Scientifique, Institut de Biologie Moléculaire et Cellulaire, Laboratoire d'Immunologie et Chimie Thérapeutiques, Unité Propre de Recherche 9021, 67000 Strasbourg, France; [d]Istituto Zooprofilattico Sperimentale della Sardegna, 07100 Sassari, Italy; [e]Infectious Disease and Immunogenetics Section, Department of Transfusion Medicine, Clinical Center and Trans-National Institutes of Health Center for Human Immunology, National Institutes of Health, Bethesda, MD 20892; and [f]Dipartimento di Oncologia, Biologia, e Genetica e Dipartimento di Medicina Interna, Universita' degli Studi di Genova, 16132 Genoa, Italy

Ultrasonography is a fundamental diagnostic imaging tool in everyday clinical practice. Here, we are unique in describing the use of functionalized multiwalled carbon nanotubes (MWCNTs) as hyperechogenic material, suggesting their potential application as ultrasound contrast agents. Initially, we carried out a thorough investigation to assess the echogenic property of the nanotubes in vitro. We demonstrated their long-lasting ultrasound contrast properties. We also showed that ultrasound signal of functionalized MWCNTs is higher than graphene oxide, pristine MWCNTs, and functionalized single-walled CNTs. Qualitatively, the ultrasound signal of CNTs was equal to that of sulfur hexafluoride (SonoVue), a commercially available contrast agent. Then, we found that MWCNTs were highly echogenic in liver and heart through ex vivo experiments using pig as an animal model. In contrast to the majority of ultrasound contrast agents, we observed in a phantom bladder that the tubes can be visualized within a wide variety of frequencies (i.e., 5.5–10 MHz) and 12.5 MHz using tissue harmonic imaging modality. Finally, we demonstrated in vivo in the pig bladder that MWCNTs can be observed at low frequencies, which are appropriate for abdominal organs. Importantly, we did not report any toxicity of CNTs after 7 d from the injection by animal autopsy, organ histology and immunostaining, blood count, and chemical profile. Our results reveal the enormous potential of CNTs as ultrasound contrast agents, giving support for their future applications as theranostic nanoparticles, combining diagnostic and therapeutic modalities.

nanomaterials | biocompatibility | nanomedicine | nanobiotechnology | echography

Carbon nanotubes (CNTs) represent a potential and emerging powerful tool in diagnostic imaging (1). O'Connell et al. first demonstrated near-infrared (NIR) photoluminescence from micelle-encapsulated CNTs (2). Following this observation, several other studies investigated CNT applications in photoluminescence imaging (3). Single-walled CNTs (SWCNTs) also exhibit high-resonance Raman scattering because of their sharp electronic density of state. This characteristic was further explored for imaging purposes in vitro and ex vivo (i.e., in hepatic cells and tissue slices) (4, 5). The use of CNTs as multicolor contrast agents for multiplexed Raman imaging has also been described (6). Recently, genetically engineered multifunctional M13 phage has been assembled with SWCNTs and detected in tissue phantoms in the second NIR window (7). Another study has reported the high potential of this type of nanomaterial for deep-tissue anatomical imaging in the second NIR window in mice (8). Moreover, pilot studies have shown the possible applications of SWCNTs conjugated with targeting peptides in photoacoustic imaging (9, 10).

Photoacoustics and ultrasonography are both powerful imaging methodologies but with substantial differences: (i) the photoacoustics induces a region of tissue to become an active acoustic source, but the conventional ultrasound introduces high-frequency acoustic waves and detects their echo; (ii) the photoacoustics is broadband, containing frequencies up to 50 MHz or more, but ultrasound usually uses a single frequency. In addition, despite the high potential of photoacoustic imaging, ultrasonography remains the most popular medical imaging modality because of to the low price per examination and safety (11). There are few important requirements for an exogenous substance to be considered an ultrasound contrast agent (USCA): (i) an easy way of administration, either in the blood pool or in a cavity; (ii) a most possible high stability; (iii) an easy elimination from the body; (iv) a low toxicity; and (v) a good echogenicity. Several studies have already shown that functionalized CNTs are endowed with the first four characteristics of a USCA. CNTs have been injected through intraperitoneal and intravenous routes in animal models; they are stable in different biological solutions and they can be eliminated by renal or hepatobiliary clearance when appropriately functionalized (1, 3). Moreover, functionalized CNTs were found to be not toxic in previous studies carried out by us (12) and others (13, 14). In light of these considerations, the present work was designed to test CNTs in conventional ultrasound imaging focusing on the assessment and characterization of their echogenic properties.

## Results

In this study we used multiwalled CNTs (MWCNTs) that were first oxidized and subsequently functionalized by 1,3-dipolar cycloaddition of azomethine ylides (ox-MWCNT-NH$_3^+$) (Fig. S1) to render them biocompatible (12, 15). These functionalized MWCNTs have a diameter of 20–30 nm and an average length of about 400 nm. For the ultrasound experiments, the nanotubes were simply added to sterile ultrapure water or homogeneously dispersed in sterile ultrapure water by bath sonication (see SI Text for details). We initially tested the echogenic property of functionalized CNTs at increasing doses without sonication treatment. Fig. 1A shows visible nanomaterial depositions at the bottom of the wells at 100 and 1,000 μg/mL. The white arrows in the corresponding ultrasound images indicate a visible and strong ultrasound signal at the highest concentrations of the tubes (Fig. 1B). The intensity of the ultrasound signal was dose-

## Functionalized MWCNT without sonication
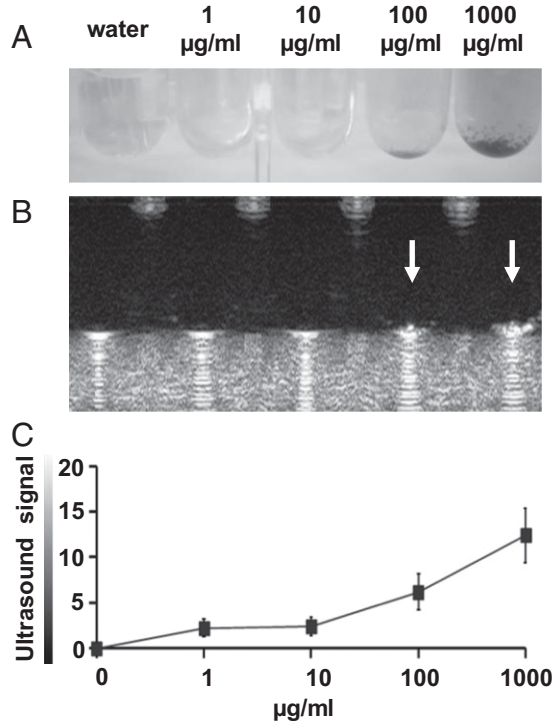


## Functionalized MWCNT after sonication
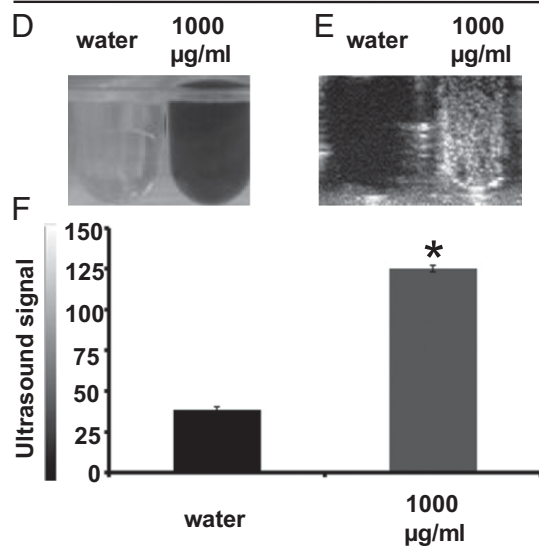


**Fig. 1.** Ultrasound detection of functionalized MWCNTs before and after sonication. (*A*) Photographs of water and MWCNTs (1–1,000 μg/mL) without applying sonication in a 96-well plate. (*B*) The corresponding ultrasound images of *A*. (*C*) Calculation of the ultrasound signal on different images (analyzed pixel = 2,928). Water was used as negative control and its signal was subtracted. (*D*) Photographs of water and MWCNTs (at 1,000 μg/mL) after the sonication process. (*E*) The corresponding ultrasound images of *D*. (*F*) Calculation of the ultrasound signal (analyzed pixel = 6,489). The ultrasound signal is reported in 8-bit gray scale intensity from 0 to 255 shades of gray recordable. Signal intensity was calculated on measurements of three investigations. The error bars represent the SD ($n = 3$); *$P < 0.05$. *A*, *B*, *D*, and *E* are representative images of three independent experiments.

dependent (Fig. 1*C*). As for biomedical uses, it is necessary to obtain highly homogenous dispersions; we then tested the echogenic properties of MWCNTs after sonication. Functionalized CNTs

became clearly highly dispersed in water (Fig. 1*D*). Dispersibility of ox-MWCNT-NH$_3^+$ was persistent; the tube dispersions were stable for several days. The white area visible in the equivalent ultrasound image suggests the high echogenicity of sonicated functionalized MWCNTs (Fig. 1*E*) The ultrasound signal in dispersed MWCNTs was three-times more intense than plain water used as negative control (38.6 vs. 125.0, respectively; $P < 0.05$) (Fig. 1*F*).

Next, we wanted to assess the ability of CNTs to produce a long-lived ultrasound signal (Fig. S2). The echogenic property of MWCNTs was significantly higher ($P < 0.05$) compared with water after more than 60 min of ultrasound irradiation; data also prove their ability to emit under continuative pulsed sounds. We then decided to compare ox-MWCNT-NH$_3^+$ with the precursor pristine nanotubes and graphene oxide (GO) (Fig. 2), an emerging form of carbon explored for biomedical applications (16) and materials science (17). All carbon nanomaterials were sonicated. Although GO can be easily dispersed using the same conditions of CNTs, only functionalized CNT dispersions in water were highly homogenous and stable (at least for more than 24 h) (Fig. 2*A*), as visible in the corresponding ultrasonography image as well (Fig. 2*B*). Image mean values in terms of gray shade demonstrate that MWCNTs generated a higher signal compared with GO (109.6 ± 6.1 *vs.* 77.6 ± 6.5, respectively; $P < 0.05$). Moreover, as expected, the signal from the functionalized CNTs after sonication treatment was more homogeneous (Fig. 2*C*). To further investigate the different types of nanotubes we have evaluated the possible differences between SWCNTs and MWCNTs in terms of echogenic properties. We performed a comparative experiment using SWCNTs oxidized and then modified by 1,3-dipolar cycloaddition of azomethine ylides as MWCNTs (Fig. S3). The image analysis showed a statistically significant difference ($P < 0.05$), indicating that the multiwalled nanotubes are more echogenic compared with the single-walled nanotubes.

To better characterize the quality of CNT signal, we compared functionalized MWCNTs with the commercially available ultrasound contrast agent SonoVue. SonoVue consists of microbubbles containing sulfur hexafluoride in a perfluorocarbon inactive gas (18). SonoVue and CNTs were both clearly echogenic (Fig. S4). From ultrasonography images (Fig. S4*A*), a nonstatistically significant difference was observed on the intensity of the ultrasound signals between sulfur hexafluoride (68.3 ± 8.5) and functionalized MWCNTs (72.6 ± 13.0), from three independent experiments (Fig. S4*B*).

Stimulated by these results, we decided to evaluate in ex vivo experiments if functionalized MWCNTs were visible by ultrasound imaging, selecting two pig organs. There are several advantages in the use of swine in biomedical and pharmaceutical research because they share with humans similar anatomic and physiologic characteristics in their cardiovascular, digestive, and urinary systems (19). A pig animal model was chosen because of these anatomic similarities to humans, when compared with other mammalian species. We first investigated if injected ox-MWCNT-NH$_3^+$ were visible in pig liver and heart on isolated organs, because these organs have different tissue characteristics (Fig. S5). Ultrasound images before and after injection of MWCNTs were acquired using water as a negative control (Fig. 3 *A* and *C*). Functionalized CNTs were injected in the organ using a dose of 300 μL at 1,000 μg/mL. The analysis of the acquired images before and after injection is shown in Fig. 3 *B* and *D*, respectively. The yellow arrows in Fig. 3 *A* and *C* indicate a wide area with high echogenic intensity because of the presence of CNTs into the injected organs. For both types of organs, we then calculated a subtraction image between the ultrasound image taken after water injections and the image taken before injection. We performed the same type of calculation for MWCNTs. Ultrasound signaling of MWCNTs was significantly higher, more than 20-times, compared with water in both the
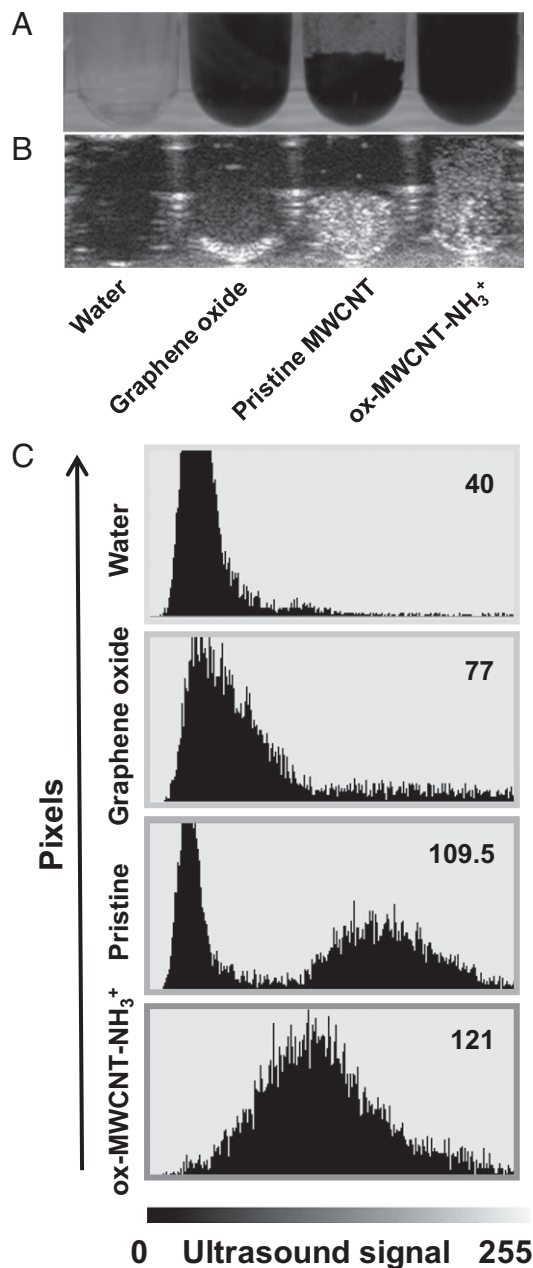
**Fig. 2.** Ultrasound comparison between GO, pristine MWCNTs, and ox-MWCNT-NH$_3^+$. (*A*) Image of GO, pristine MWCNTs, and ox-MWCNT-NH$_3^+$ (at 1,000 µg/mL) in a 96-well plate. (*B*) The corresponding ultrasound image of *A*. (*C*) Graphs derived from the image analysis (analyzed pixel = 6,962). The ultrasound signal in *y* axis dimension is expressed in gray shade value based on 8-bit scale intensity from 0 to 255. Mean intensity reported for all samples (top right numbers in each panel) are representative of three investigations.

transfer (22). On the basis of the high similarity between CNTs and graphite, we can conclude that the difference in signal values for CNTs (with high acoustic impedance) compared with the ultrasounds produced by the tissues (with low acoustic impedance) was clearly a result of the intrinsic chemico-physical properties (24) of the nanotubes, as also observed in Fig. 2. The actual mechanism with which CNTs generate the acoustic signal is not known and requires further investigation. We can exclude, for example, that the signal derives from the liberation of small bubbles entrapped in the inner space of the nanotubes (i.e., there was no difference using degassed or nondegassed samples). On the other hand, we cannot rule out that functionalized CNTs behave as the center of nucleation of air bubbles, eventually leading to an intense echogenic signal.

In view of the results obtained from the ex vivo experiments using CNTs (Fig. 3), we decided to compare functionalized MWCNTs to SonoVue in liver and heart (Fig. S6). The primary application of SonoVue is aimed at the characterization of focal liver lesions (25). We confirmed the results in solution (Fig. S4) by quantifying the ultrasound responses in both the liver and heart (Fig. S6). Although we found a statistically significant difference between SonoVue and MWCNTs in the heart (Fig. S6 *C and D*), the echogenic signals in the liver were of the same intensity, supporting the potential use of functionalized CNTs for imaging this type of organ (Fig. S6 *A and B*). To date, the large
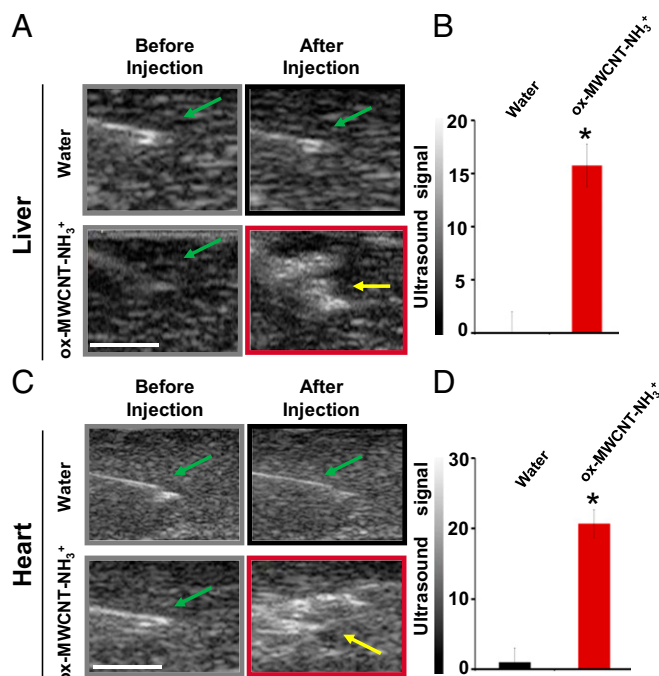


**Fig. 3.** Ultrasound detection of functionalized MWCNTs ex vivo in liver and heart from pigs. (*A and C*) Ultrasound images of liver and heart. In gray and black rectangles (*Upper*) are represented the images before and after injection of 300 µL water; in gray and red rectangles (*Lower*) are represented the images before and after injection of 300 µL of functionalized MWCNTs at 1,000 µg/mL concentration. Green arrow indicates the tip of syringe before injection. Yellow arrow indicates a higher ultrasound signal after injection of MWCNTs. (Scale bars, 5 mm.) (*B and D*) Signal analysis in liver and heart after the echogenicity subtraction of images before injection, for water and MWCNTs (*$P < 0.01$) (analyzed pixel: liver = 30,810; heart = 26,880). Ultrasound signal is reported in 8-bit gray scale intensity from 0 to 255 shades of recordable gray. Ultrasound signal was calculated on measurements of experiments performed in three different livers and three hearts from healthy pigs. The error bars represent SD (*n* = 3). Ultrasound images are representative data of three investigations.

liver and heart (*$P < 0.05$). MWCNTs consist of rolled up concentric graphene layers, like in graphite sheets. The chemical nature of CNTs is very similar to graphite. It is reported in the literature that graphite has an acoustic impedance of 2.71 Mrayl (20), which is much higher than that of organs such as liver and heart (1.64 and 1.75 Mrayl, respectively) (21). Moreover, graphite has mechanical properties in terms of density (ρ) and velocity of sound (*c*) ($\rho_g = 2267$ kg·m$^{-3}$, $c_g = 18,350$ m·s$^{-1}$) that strongly differ from those of biological tissues ($\rho_{biol} \sim 1,000$ kg·m$^{-3}$, $c_{biol} \sim 1500$ m·s$^{-1}$) (22, 23). For its acoustic properties, graphite has been previously investigated as an ultrasonic transcutaneous energy

majority of USCAs can only be used at frequencies < 5 MHz; as such, there is an increasing interest in extending contrast imaging to high frequencies useful for superficial tissue, such as carotid and breast (26, 27). For this reason, we would like to emphasize that for all data reported above, we did ultrasound scans using a 12.5-MHz frequency, applying the tissue harmonic imaging (THI) modality. To investigate if MWCNTs were detectable without THI and at different frequencies, we used a bladder phantom (Fig. S7). CNTs, first injected in the bladder phantom and detected at 12.5 MHz in THI modality, were bright and evident (Movie S1). Without THI CNTs were hardly visible at 12.5 MHz. However, reducing the frequencies, without using THI, the nanotubes were again clearly recognizable at 10, 8, and 5.5 MHz (Fig. S7).

As a last step, we decided to move to in vivo experiments, focusing on swine bladder as example of an abdominal organ in terms of depth into the body. We again used pigs as an animal model because swine is an ideal model this purpose as well (28). Female healthy pigs were anesthetized with azaperone (Fig. S8) (see *SI Text* for details). Then we performed an intravesical administration of MWCNTs (Fig. 4) under ultrasound guide. ox-MWCNT-NH$_3^+$ were used at a concentration of 1,000 μg/mL, one of the highest doses used on animal models that, for example, has not provoked detectable effect on mice (29). Fig. 4A displays the pig bladder before MWCNT injection. In Fig. 4B we show a wide echogenic area recovered after completed nanotube injection. These in vivo data confirmed the results obtained in vitro and ex vivo in liver and heart. We have to emphasize that for this experiment we used a convex probe (2.5–5 MHz), proving that the wide variety of frequencies with functionalized MWCNTs can be visualized, with the possibility of using them for superficial and abdominal organs. A urine sample after bladder injection with MWCNTs were collected and analyzed by transmission electron microscopy (TEM) (Fig. S9). TEM images show MWCNTs in pig urine, proving that this nanomaterial was easily eliminated. In addition, to confirm that functionalized MWCNTs can be used with different routes of administration, we investigated their echogenicity property on whole pig blood ex vivo (Fig. S10) and in vivo by intravenous injection (Movie S2). We observed that MWCNTs were clearly detectable in blood. In Movie S2 the CNTs are clearly visible during the injection in the anterior vena cava as bright white spots (see bottom right side of the movie and Fig. S11). Based on several factors supporting the idea that pigs represent the ideal model and meet the challenges of future emerging technologies and toxicology (30), we investigated the possible toxic effects of MWCNTs after injection (see *SI Text* for details). An autopsy after 7 d on the animals did not reveal any sign of illness. In particular, the bladder post mortem appeared to be in normal condition (Fig. S12). Histology and immunophenotypic characterization of inflammatory cells was performed on kidney and bladder (Fig. 5). Histological investigation indicated no kidney and bladder inflammation or necrosis (Fig. 5A). In immunohistochemistry assays, no CD3$^+$ and CD79$^+$ cells were observed in the urinary bladder's wall and renal papilla, and few CD163 macrophages were present in the mucosa of the bladder, as commonly observed in healthy pigs (Fig. 5B). Histology was also performed on the liver, renal cortex, lung, and heart (Fig. S13). Again, MWCNTs did not exert adverse effects on these organs. Furthermore, the analysis of blood, including complete blood count and chemical profile, before the experiments and after 1 wk following ultrasonography, indicated that blood values were in normal range after MWCNT bladder injection (Table S1). Our data confirm previous studies showing that CNTs, appropriately functionalized, are nontoxic both in vitro toward different cell types and in vivo in mouse models (12, 29, 31, 32). The main purpose of the overall study was to investigate functionalized MWCNTs as USCAs. The acquired toxicity data were
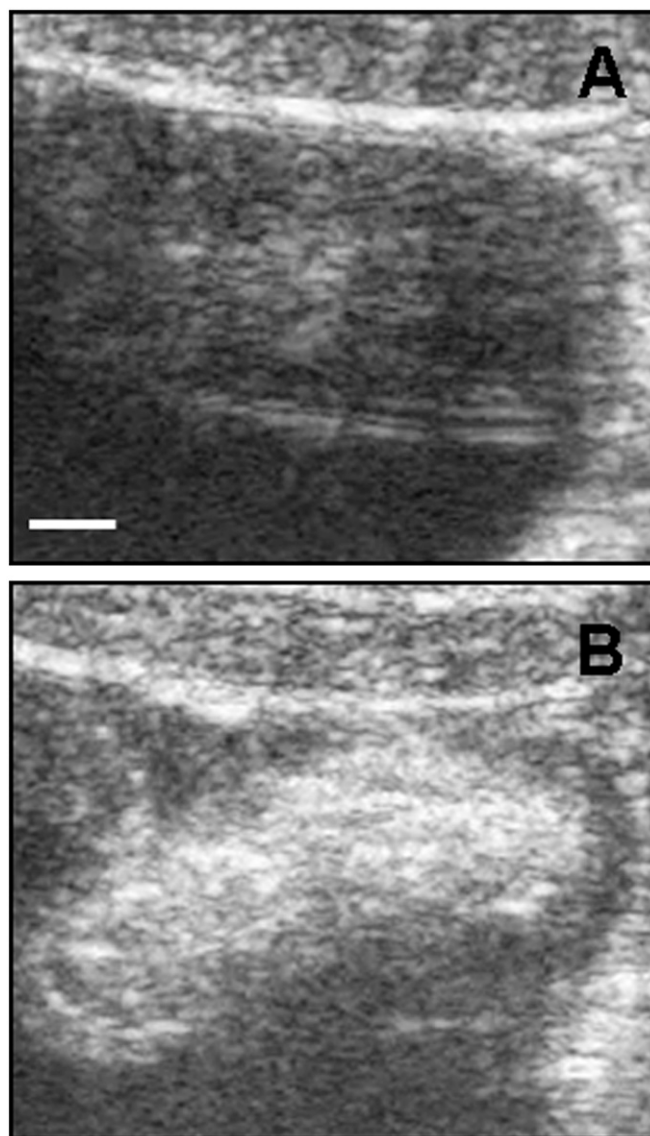


**Fig. 4.** Ultrasound detection of functionalized MWCNTs in vivo. (A) Bladder ultrasound detection before MWCNT injection. (B) MWCNTs were injected into the bladder (5 mL, at 1,000 μg/mL concentration). The images are representative results of two investigations in healthy pigs. (Scale bar, 5 mm.)

aimed only to prove the biocompatibility of CNTs used in these experiments. Obviously, in the future, it will be appropriate to perform additional experiments on the impact of CNTs in swine using a higher number of animals with additional time points of analysis and reduced doses of nanotubes.

## Discussion

Pilot studies reported the applications of CNTs as photoacoustic imaging agents (9, 10). Photoacoustic imaging is currently a hot topic in scientific research but, according to Wang and Hu, we have to remember that clinical systems need to pass rigorous validations, and photoacoustic imaging has just started being used in humans (33). Because the technique itself needs to pass further proof for applications in every day clinical practice, it may be difficult, in the near future, to image CNTs as photoacoustic agents. Ultrasonography is instead a low-cost imaging tool widely used in clinic diagnosis and with an old history in medicine. We have demonstrated that functionalized CNTs can
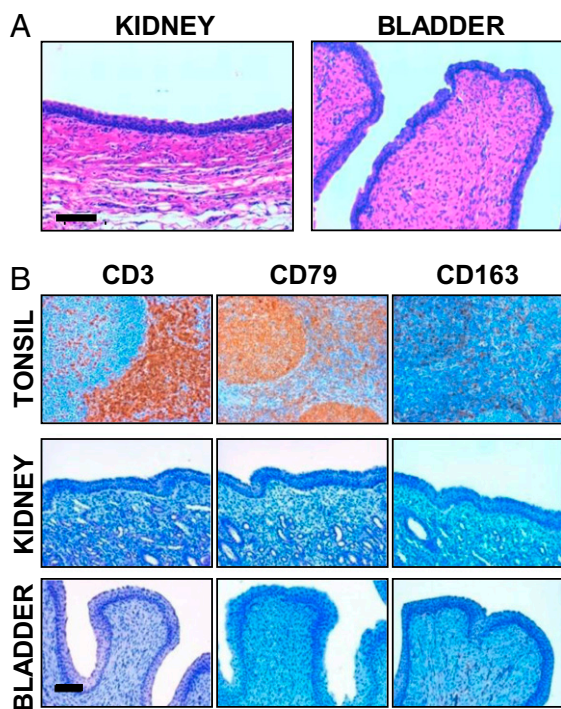
**Fig. 5.** Histology and immunohistochemistry of kidney and bladder. (*A*) Paraffin-embedded sections stained with H&E of kidney (renal papilla) and bladder after 7 d from the MWCNT injection. The images are representative results of three investigations. (Scale bar, 100 μm.) (*B*) Inflammatory cell immunophenotyping in serial paraffin-embedded sections of urinary bladder and kidney, at the inner zone of the medulla (papilla). CD3, CD79, and CD163 were used as markers for T and B lymphocytes and activated macrophages, respectively. A normal swine palatine tonsil is also shown as positive control. Immune reactions were visualized by 3,3′-diaminobenzidine chromogen, Mayer's hematoxylin counterstaining. The images are representative results of three investigations. (Scale bar, 100 μm.)

be developed as promising and suitable materials for ultrasound imaging, having all necessary characteristics of a regular USCA. In addition, CNTs may have additional advantages toward very promising possibilities for the future of ultrasonography. The size of the majority microbubble-based ultrasound contrast agent (1–8 μm) renders them purely intravascular flow tracers. In contrast, the chemico-physical characteristics of CNTs (i.e., 400 nm in length in the present study), make them potentially able to extravasate and reach a tumor region, which can exhibit a vascular pore size up to 780 nm (34). The small size of CNTs will be of great advantage, considering their ability to cross the endothelial barriers and, as targetable materials, to reach a tumor region, at the same time being vehicles for therapeutic agents (1, 3). USCAs are classified as long half-life agents when the signal persists for more than 5 min after an intravenous bolus injection (35). Most of the USCAs are eliminated in few minutes through the lungs. We previously observed functionalized CNT blood clearance in mice at 3 h postinjection (36). This finding suggests the possibility to use CNTs in case of long ultrasonography investigations eventually associated with therapeutic purposes. Within this context, few pilot studies have proposed the combination of microbubble USCAs with a therapeutic load or with targeting compounds (37–39). Research focusing on microbubbles as a drug delivery system and targetable compounds is rather limited and at an early stage of development, compared with the literature proposing CNTs as drug-delivery systems (3, 40–42). In addition, little work has been carried out on other types of nanomaterials and nanoparticles, including silica nanoparticles (43), iron oxide nanoparticles (44), and PEGylated nanocapsules (45) as possible ultrasound contrast

agents. Aside from these studies, and keeping in mind possible future developments of nanoparticles acting as USCAs being able to target specific cells and deliver a drug, CNTs remain one of the most promising nanomaterials because of their extremely high aspect ratio (length/diameter ratio) and their easy capacity to penetrate cell membranes without exerting toxic effects. In addition, the possibility to link to the nanotubes different molecules in a multifunctional approach and in a precise chemical-controlled manner (46) is also another characteristic that is being considered for future construction of multimodal nanomaterials. Indeed, multifunctionalized CNTs can offer both imaging and therapeutic capabilities. The new field of theranostics concerns the development of materials with concurrent and complementary therapeutic and diagnostic features (47). On the basis of the echogenic property that we have devised in the present work, it will be highly beneficial for the future development of functionalized CNTs as new targeted ultrasound contrast agents combined with therapeutic compounds.

In summary, we have shown that functionalized MWCNTs can be imaged in ultrasonography. A time course using continuative ultrasounds proved that the echogenic property is not affected by ultrasound irradiation. We have demonstrated that MWCNTs display a high signal compared with GO, pristine, and functionalized single-walled nanotubes. The signal emitted from this type of tube is not different, in terms of brightness, from the common contrast agent SonoVue. We also assessed the echogenic property of MWCNTs ex vivo in the liver and heart. We have shown that, in contrast to the majority of current USCAs, CNTs were well visible at high frequencies that are advantageous for imaging superficial tissues. Finally, we have performed an in vivo intravesical MWCNT injection using a convex probe that works at low frequencies, from 2.5 to 5 MHz. Our nanomaterials were clearly visible in the bladder, proving that functionalized MWCNTs can be seen as very versatile USCAs in terms of useable frequencies. Animal autopsy, histology, immunostaining, blood counts, and chemical profile supported that CNTs did not affect the pig's health. We would like to point out, however, that the toxicity of CNTs is still an important issue, not completely solved (48–51). Concerns about the biocompatibility of nanocarbons are under debate. As a key point, a clear distinction needs to be made between the behavior of functionalized CNTs and pristine nanotubes in terms of health impact, with a favorable outcome in the case of the former (1, 3).

We expect that the proof-of-concept on the echogenic property of functionalized MWCNTs described in this work will allow future studies focused on CNTs as ideal theranostic nanoparticles, combining the following features: targetable materials, drug carriers, drug delivery enhancers, and ultrasound contrast agents.

## Materials and Methods

**Carbon Materials.** MWCNTs (20–30 nm diameter, 0.5–2 μm length, 95% purity; batch 1240XH) were purchased from Nanostructured and Amorphous Materials. Pristine nanotubes were initially oxidized to obtain ox-MWCNTs and subsequently submitted to the 1,3-dipolar cycloaddition reaction to generate positively charged ammonium functionalized ox-MWCNT-NH$_3^+$, as previously described (12). GO (batch GO.Z-10.2–12) was purchased from NanoInnova Technologies. HiPCO SWCNTs were purchased from Carbon Nanotechnologies (lot R0496). Pristine nanotubes were initially oxidized to obtain ox-SWCNTs (52) and subsequently submitted to the 1,3-dipolar cycloaddition reaction to generate positively charged ammonium functionalized ox-SWCNT-NH$_3^+$; the synthesis procedure and characterization were the same as the multiwalled nanotubes. Details on the preparation of the carbon nanomaterial dispersions and TEM analysis are reported in *SI Text*.

**Ultrasound Imaging.** Technos MPX (Esoate) was used for all of the experiments (B mode). Images in Figs. 1 and 2, and Figs. S2 and S3 were recorded with a 7.5- to 12-MHz linear probe; the instrument was set in conventional ultrasound modality (B mode), THI mode, depth 31 mm, gain 255, −1.3 dB, and mechanical index 0.9. Contrast tuned imaging (CnTi) software (Esoate) was used to analyze the signal coming from the SonoVue (Bracco) in Figs. S4 and S6. Data for MWCNTs illustrated in Fig. S6 were recorded with an instrument

set in B mode, CnTi in fundamental imaging, depth 31 mm, gain 130, and mechanical index 0.071. Images in Fig. 3 were recorded with a 7.5- to 12-MHz linear probe; the instrument was set in B mode, THI, depth 21 mm, gain 225, −1.3 dB, and mechanical index 1.0. The experiment in Fig. 4 was performed using a 2.5- to 5-MHz convex probe; the instrument was set in B mode, THI, depth 77 mm, gain 155, −1.4 dB, and mechanical index 0.7. The experiment displayed in Fig. S10 was performed using a 7.5- to 12-MHz linear probe; the instrument was set in B mode, THI, depth 21 mm, gain 255, −1.3 dB, and mechanical index 1.0. In all ultrasound experiments the probe was placed above the examined sample and oriented perpendicular to the plate, organ, or phantom bladder (see also Fig. S5 for the injection modality into ex vivo organs). To exclude that possible air bubbles, present in the dispersions of the nanotubes, might generate an echogenic signal, an ultrasonography experiment with water-degassed samples was performed. Movie S1 was recorded with a 7.5- to 12-MHz linear probe in B mode, THI, depth 41 mm, gain 170, −1.3 db and 0.9 of mechanical index. Movie S2 was recorded using a 7.5- to 12-MHz linear probe; the instrument was set in B mode, THI, depth 41 mm, gain 150, −1.3 dB, and mechanical index 1.8. Details on the ultrasound image analysis, animal procedures, histopathology and immunophenotypic characterization, and statistics are reported in SI Text.

1. Kostarelos K, Bianco A, Prato M (2009) Promises, facts and challenges for carbon nanotubes in imaging and therapeutics. *Nat Nanotechnol* 4:627–633.
2. O'Connell MJ, et al. (2002) Band gap fluorescence from individual single-walled carbon nanotubes. *Science* 297:593–596.
3. Liu Z, Tabakman S, Welsher K, Dai H (2009) Carbon nanotubes in biology and medicine: In vitro and in vivo detection, imaging and drug delivery. *Nano Res* 2:85–120.
4. Heller D, Baik S, Eurell T, Strano M (2005) Single-walled carbon nanotube spectroscopy in live cells: Towards long-term labels and optical sensors. *Adv Mater* 17:2793–2799.
5. Liu Z, et al. (2008) Circulation and long-term fate of functionalized, biocompatible single-walled carbon nanotubes in mice probed by Raman spectroscopy. *Proc Natl Acad Sci USA* 105:1410–1415.
6. Liu Z, et al. (2008) Multiplexed multicolor Raman imaging of live cells with isotopically modified single walled carbon nanotubes. *J Am Chem Soc* 130:13540–13541.
7. Yi H, et al. (2012) M13 phage-functionalized single-walled carbon nanotubes as nanoprobes for second near-infrared window fluorescence imaging of targeted tumors. *Nano Lett* 12:1176–1183.
8. Welsher K, Sherlock SP, Dai H (2011) Deep-tissue anatomical imaging of mice using carbon nanotube fluorophores in the second near-infrared window. *Proc Natl Acad Sci USA* 108:8943–8948.
9. de la Zerda A, et al. (2010) Ultrahigh sensitivity carbon nanotube agents for photoacoustic molecular imaging in living mice. *Nano Lett* 10:2168–2172.
10. De la Zerda A, et al. (2008) Carbon nanotubes as photoacoustic molecular imaging agents in living mice. *Nat Nanotechnol* 3:557–562.
11. Postema M, Gilja OH (2011) Contrast-enhanced and targeted ultrasound. *World J Gastroenterol* 17:28–41.
12. Delogu LG, et al. (2012) Ex vivo impact of functionalized carbon nanotubes on human immune cells. *Nanomedicine (Lond)* 7:231–243.
13. Schipper ML, et al. (2008) A pilot toxicology study of single-walled carbon nanotubes in a small sample of mice. *Nat Nanotechnol* 3:216–221.
14. Wu P, et al. (2008) Biocompatible carbon nanotubes generated by functionalization with glycodendrimers. *Angew Chem Int Ed Engl* 47:5022–5025.
15. Bianco A, Kostarelos K, Prato M (2011) Making carbon nanotubes biocompatible and biodegradable. *Chem Commun (Camb)* 47:10182–10188.
16. Feng L, Liu Z (2011) Graphene in biomedicine: Opportunities and challenges. *Nanomedicine (Lond)* 6:317–324.
17. Wan X, Huang Y, Chen Y (2012) Focusing on energy and optoelectronic applications: A journey for graphene and graphene oxide at large scale. *Acc Chem Res* 45:598–607.
18. Hu YZ, Zhu JA, Jiang YG, Hu B (2009) Ultrasound microbubble contrast agents: Application to therapy for peripheral vascular disease. *Adv Ther* 26:425–434.
19. Swindle MM, Makin A, Herron AJ, Clubb FJ, Jr., Frazier KS (2012) Swine as models in biomedical research and toxicology testing. *Vet Pathol* 49:344–356.
20. Inficon. (2012) List of the density and acoustic impedance values for commonly used materials. Available at www.inficonthinfilmdeposition.com/en/densityandacousticvalues.html. Accessed September 13, 2012.
21. Ozeri S, Shmilovitz D (2010) Ultrasonic transcutaneous energy transfer for powering implanted devices. *Ultrasonics* 50:556–566.
22. Mari JM, Cachard C (2011) Ultrasonic scanning of straight micro tools in soft biological tissues: Methodology and implementation. *Ultrasonics* 51:632–638.
23. Matsukawaa M, Akimoto T, Ueba S, Otania T (2002) Ultrasonic wave properties in the particle compounded agarose gels. *Ultrasonics* 40(1–8):323–327.
24. Jafari SB, Khadem SE, Malekfar R (2012) A comprehensive study of sound pressure in a finite-length fluid-filled multi-walled carbon nanotube. *Ultrasonics* 52:655–662.
25. Cabassa P, Bipat S, Longaretti L, Morone M, Maroldi R (2010) Liver metastases: Sulphur hexafluoride-enhanced ultrasonography for lesion detection: A systematic review. *Ultrasound Med Biol* 36:1561–1567.
26. Wilson SR, Burns PN (2010) Microbubble-enhanced US in body imaging: What role? *Radiology* 257:24–39.
27. Helfield BL, Cherin E, Foster FS, Goertz DE (2012) Investigating the subharmonic response of individual phospholipid encapsulated microbubbles at high frequencies: A comparative study of five agents. *Ultrasound Med Biol* 38:846–863.
28. Vodicka P, et al. (2005) The miniature pig as an animal model in biomedical research. *Ann N Y Acad Sci* 1049:161–171.
29. Lacerda L, et al. (2008) Tissue histology and physiology following intravenous administration of different types of functionalized multiwalled carbon nanotubes. *Nanomedicine (Lond)* 3:149–161.
30. Forster R, Bode G, Ellegaard L, van der Laan JW; Steering Group of the RETHINK Project (2010) The RETHINK project—Minipigs as models for the toxicity testing of new medicines and chemicals: An impact assessment. *J Pharmacol Toxicol Methods* 62:158–159.
31. Dumortier H, et al. (2006) Functionalized carbon nanotubes are non-cytotoxic and preserve the functionality of primary immune cells. *Nano Lett* 6:1522–1528.
32. Firme CP, 3rd, Bandaru PR (2010) Toxicity issues in the application of carbon nanotubes to biological systems. *Nanomedicine* 6:245–256.
33. Wang LV, Hu S (2012) Photoacoustic tomography: In vivo imaging from organelles to organs. *Science* 335:1458–1462.
34. Hobbs SK, et al. (1998) Regulation of transport pathways in tumor vessels: Role of tumor type and microenvironment. *Proc Natl Acad Sci USA* 95:4607–4612.
35. Correas JM, et al. (2001) Ultrasound contrast agents: Properties, principles of action, tolerance, and artifacts. *Eur Radiol* 11:1316–1328.
36. Singh R, et al. (2006) Tissue biodistribution and blood clearance rates of intravenously administered carbon nanotube radiotracers. *Proc Natl Acad Sci USA* 103:3357–3362.
37. Lentacker I, et al. (2009) Ultrasound exposure of lipoplex loaded microbubbles facilitates direct cytoplasmic entry of the lipoplexes. *Mol Pharm* 6:457–467.
38. Rapoport N, Gao Z, Kennedy A (2007) Multifunctional nanoparticles for combining ultrasonic tumor imaging and targeted chemotherapy. *J Natl Cancer Inst* 99:1095–1106.
39. Sanna V, et al. (2011) Development of polymeric microbubbles targeted to prostate-specific membrane antigen as prototype of novel ultrasound contrast agents. *Mol Pharm* 8:748–757.
40. Delogu LG, et al. (2009) Conjugation of antisense oligonucleotides to PEGylated carbon nanotubes enables efficient knockdown of PTPN22 in T lymphocytes. *Bioconjug Chem* 20:427–431.
41. Herrero MA, et al. (2009) Synthesis and characterization of a carbon nanotube-dendron series for efficient siRNA delivery. *J Am Chem Soc* 131:9843–9848.
42. Liu Z, et al. (2008) Drug delivery with carbon nanotubes for in vivo cancer treatment. *Cancer Res* 68:6652–6660.
43. Casciaro S, et al. (2010) Optimal enhancement configuration of silica nanoparticles for ultrasound imaging and automatic detection at conventional diagnostic frequencies. *Invest Radiol* 45:715–724.
44. Xu B, et al. (2011) "Two-in-one" fabrication of Fe3O4/MePEG-PLA composite nanocapsules as a potential ultrasonic/MRI dual contrast agent. *Langmuir* 27:12134–12142.
45. Díaz-López R, et al. (2010) The performance of PEGylated nanocapsules of perfluorooctyl bromide as an ultrasound contrast agent. *Biomaterials* 31:1723–1731.
46. Prato M, Kostarelos K, Bianco A (2008) Functionalized carbon nanotubes in drug design and discovery. *Acc Chem Res* 41:60–68.
47. Jokerst JV, Gambhir SS (2011) Molecular imaging with theranostic nanoparticles. *Acc Chem Res* 44:1050–1060.
48. Colvin VL (2003) The potential environmental impact of engineered nanomaterials. *Nat Biotechnol* 21:1166–1170.
49. Poland CA, et al. (2008) Carbon nanotubes introduced into the abdominal cavity of mice show asbestos-like pathogenicity in a pilot study. *Nat Nanotechnol* 3:423–428.
50. Nagai H, et al. (2011) Diameter and rigidity of multiwalled carbon nanotubes are critical factors in mesothelial injury and carcinogenesis. *Proc Natl Acad Sci USA* 108:E1330–E1338.
51. Miyako E, et al. (2012) Photothermal regulation of gene expression triggered by laser-induced carbon nanohorns. *Proc Natl Acad Sci USA* 109:7523–7528.
52. Li S, et al. (2008) Adsorption of carbon nanotubes on active carbon microparticles. *Carbon* 46:1091–1095.

MEDICAL SCIENCES

CHEMISTRY